Nano Research

Open Access

Research Article

Zwitterionic hyaluronic acid derivatives for co-delivery of both chemotherapeutic and nucleic acid drugs in breast cancer treatment

Ruo-Lin Jiang[1,6,§], Hui-Na Liu[1,§], Yu-Fan Yang[1], Zhi-Cheng Zhang[2], Qi Dai[1,2], Xiao-Yan Bao[1], Lin-Jie Wu[1], Ya-Xin Qin[1], Xin Tan[1], Xiao-Yan Sun[1], Xu-Fang Ying[1,6], Zhi-Qing Ben[1], and Min Han[1,2,3,4,5] ✉

[1] *Institute of Pharmaceutics, College of Pharmaceutical Sciences, Zhejiang University, Hangzhou 310058, China*
[2] *Department of Radiation Oncology, Key Laboratory of Cancer Prevention and Intervention, The Second Affiliated Hospital, College of Medicine, Zhejiang University, Hangzhou 310058, China*
[3] *Hangzhou Institute of Innovative Medicine, Zhejiang University, Hangzhou 310058, China*
[4] *Jinhua Institute of Zhejiang University, Jinhua 321299, China*
[5] *National Key Laboratory of Advanced Drug Delivery and Release Systems, Zhejiang University, Hangzhou 310058, China*
[6] *Polytechnic institute, Zhejiang University, Hangzhou 310015, China*
[§] *Ruo-Lin Jiang and Hui-Na Liu contributed equally to this work.*

Cite this article: *Nano Research*, **2025**, *18*, 94907076. https://doi.org/10.26599/NR.2025.94907076

ABSTRACT: Traditionally, hyaluronic acid has been widely used for drug delivery, but the current application bottleneck is that hyaluronic acid is hydrophilic and electronegative, which makes it difficult to carry hydrophobic drugs and small interfering RNA (siRNA) with the same charge. Based on previous studies, we designed and synthesized hyaluronic acid nanocarriers HA-spermine/*N,N,N*-trimethylcystamine/DOX-TPP (HSTD) for loading siRNA to overcome the problem of siRNA release caused by strong electrostatic interaction. Then, *N,N,N*-trimethylcystamine in the carrier can be degraded by intracellular glutathione to completely and rapidly release siRNA, thus promoting transfection. Moreover, when co-delivered with the chemotherapy drug doxorubicin (DOX), this novel nanocarrier showed promising synergy in inhibiting tumor growth.

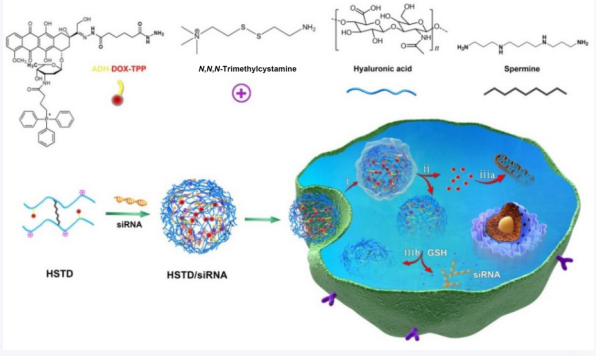

KEYWORDS: zwitterionic hyaluronic acid, *N,N,N*-trimethylcystamine, small interfering RNA (siRNA), doxorubicin

1 Introduction

Hyaluronic acid (HA) is a linear polysaccharide, consisting of N-acetyl-D-glucosamine and D-glucuronic acid. As widely distributed in the extracellular matrix of most tissues, HA is water-soluble, biocompatible, biodegradable, non-immunogenic, and non-inflammatory. In addition, the specific receptor of hyaluronic acid, CD44, is overexpressed on the surface of various malignant tumor cells [1, 2]. There are various active groups in the structure of HA, which can be physically or chemically modified to prepare derivatives that can be used as good carrier materials for drug delivery. Over the past decade, HA and its derivatives have been used to deliver proteins [3], nucleic acids [4], and anti-tumor drugs [5]. It has proved that HA can be used as a kind of sustained-release carrier for drugs, which can delay drug release and prolong drug efficacy.

However, the application of HA in drug delivery, especially nucleic acid drugs, is still insufficient. For example, the large number of carboxyl and hydroxyl groups in the structure endows HA with strong hydrophilicity, which makes it difficult to physically encapsulate hydrophobic small molecule drugs [6]. Then, negatively charged HA makes it hard to adsorb nucleic acid drugs with the same charge, and it is necessary to introduce cationic polymers, such as polyethyleneimine (PEI) for adsorption [7, 8]. Even so, the introduction of cationic polymers makes the carrier difficult to degrade, which changes the basic properties of HA, such as the *in vivo* biocompatibility and tumor-targeting ability.

At the same time, it is well known that drug resistance is a major obstacle to effective cancer chemotherapy, and the Twist1 transcription factor is involved in epithelial-mesenchymal transition (EMT) and gives rise to chemoresistance. Therefore, delivering

Received: April 22, 2024; **Revised:** September 28, 2024
Accepted: October 17, 2024

✉Address correspondence to hanmin@zju.edu.cn

chemotherapeutics simultaneously with siRNA-inactivating Twist1 signaling pathways that are involved in the development of MDR phenotype would provide an effective approach to inhibit drug resistance and increase chemotherapy efficacy [9]. However, it remained a challenge to develop a single vector that incorporates both anionic siRNA and an amphiphilic chemotherapeutic agent, i.e. a doxorubicin (DOX) derivative targeting mitochondria that was achieved by triphenylphosphonium (TPP) conjugation (DOX-TPP), in a single nanocarrier to address various extracellular and intracellular critical barriers [10, 11].

Therefore, on the one hand, aiming at the bottleneck of HA for loading nucleic acid drugs, a small cationic molecule *N,N,N*-trimethylcystamine, which is responsive to glutathione (GSH), was synthesized to modify the basic skeleton of HA nanocarrier (HA-spermine), thereby constructing a zwitterionic HA biomaterial, which can adsorb nucleic acid drugs through the positive charge on the skeleton of HA and protect nucleic acid from degradation during the *in vivo* circulation. On the other hand, we considered using the negatively charged carboxyl group on the structure of HA-spermine to link mitochondria-targeting chemotherapy drug DOX via pH-responsive hydrazone bonds to obtain drug-carrying hyaluronic acid HA-spermine/*N,N,N*-trimethylcystamine/DOX-TPP (HSTD), which can respond to drug release by acid in the tumor microenvironment. Furthermore, stimulus-responsive structural fracture occurs in tumor cells, thereby rapidly and completely releasing nucleic acid and chemotherapy drugs to exert their efficacy (Scheme 1). Therefore, compared with traditional HA-PEI, HSTD has advantages such as good material biocompatibility and more efficient nucleic acid delivery.

2 Experimental

2.1 Materials

Hyaluronic acid (HA, M_W 48 kDa) was purchased from Zhengda Freda Co. (Jinan, China). DOX was obtained from Zhejiang Hisun Pharmaceutical Co. Ltd. (Zhejiang, China). (3-Carboxypropyl) triphenylphosphonium bromide (TPP), Spermine, polyethyleneimine (PEI, M_W 25 kDa, branched), 1-ethyl-3-(3-dimethylaminopropyl) carbodiimide hydrochloride (EDC), *N,N'*-Dicyclohexylcarbodiimide (DCC), and *N*-hydroxysuccinimide (NHS) were purchased from Sigma-Aldrich (St. Louis, MO, USA). Cystamine dihydrochloride, methyl iodide, Di-tert-butyl pyrocarbonate (Diboc), dithiothreitol (DTT), glutathione reduced ethyl ester (GSH-Oet) were purchased from Aladdin Co. (Shanghai, China). Lysotracker blue, MitoTracker Green FM, and NucBlue live cell stain Hoechst 33342 kit were purchased from Life Technologies Corporation (Carlsbad, CA, USA). 2-Butyl(4-aminohexyl)-6-(dimethylamino)-1H-benz[de]isoquinoline-1,3(2H)-dione was kindly provided by Dr. Xin Li (Zhejiang University, China). The sequence of Twist-siRNA is GCAAGAUUCAGACCCUCAATT (siTwist-1), GAUGGCAAGCUGCAGCUAUTT (siTwist-2), GGUACAUCGACUUCCUCUATT (siTwist-3) and equivalent mixture of siTwist-1, siTwist-2 and siTwist-3 (siTwist-4), scramble siRNA, FAM-labeled negative control siRNA and siRNA targeting Twist (siTwist) were synthesized by Shanghai Genepharma Co., Ltd (Shanghai, China). All other chemicals were analytical grade.

2.2 Cells and animals

MCF-7/ADR cells were purchased from Nanjing KeyGen Biotech Co., Ltd (Nanjing, China), and were cultured in RPMI 1640's Medium supplemented with 100 U/mL penicillin, 100 mg/mL streptomycin, and 10% fetal bovine serum (Gibco Life Technologies Co., Carlsbad, USA) at 37 °C using a humidified 5% CO_2 incubator (HF151UV, Heal Force, HK). Female BALB/c nude mice (18 ± 2 g) were purchased from Slaccas (Shanghai, China) and maintained under standard housing conditions. All care and handling of animals were performed according to the guidelines of the animal ethics committee of Zhejiang University (Hangzhou, China).

2.3 Synthesis of *N,N,N*-trimethylcystamine

Cystamine dihydrochloride (200 mg) was alkalified by

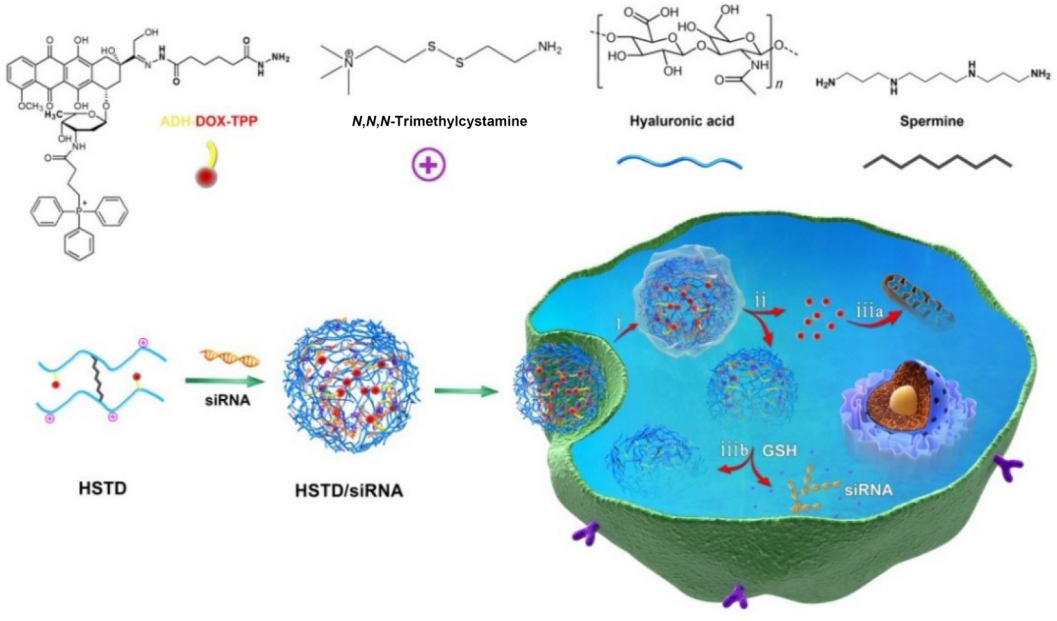

Scheme 1 Schematic illustration to show the structure of HSTD/siRNA and transport in tumor cells for synergistic therapy. i: endocytosis of HSTD/siRNA complex into tumor cells; ii: acid-mediated DOX-TPP release and escape of HSTD/siRNA from endosome; iiia: mitochondrial delivery of DOX-TPP to induce apoptosis; iiib: GSH-triggered disruption of a disulfide-based cation (i.e. *N,N,N*-trimethylcystamine) in the complex and subsequent release of siRNA for silencing Twist expression.

Triethylamine (386 μL) in 10 mL methanol. 2 mL di-tert-butyl dicarbonate ester (BOC) in 2 mL methanol was added dropwise to the cystamine dihydrochloride alkalified solution and reacted for 30 min at room temperature. After evaporation, 50 mL NaH_2PO_4 (1 M) was added to dissolve the products and was washed twice with ether to remove Di-BOC-cystamine. Then the remaining solution was basified (pH = 9) with NaOH (1 M) and extracted with EtOAc. After evaporation, white Mono-BOC-cystamine was obtained and 50 mg of them were dissolved in 1 mL acetonitrile added with K_2CO_3 (64.6 mg) and methyl iodide (73 μL), and stirred for 3 day at room temperature. The mixture was centrifuged to remove K_2CO_3 and evaporated to get the crude products. Washed twice with ether, the white *N,N,N*-trimethyl-cystamine-BOC was obtained and dissolved in 1 mL methanol, and reacted with 1 mL trifluoroacetic acid for 2 h followed by evaporation, and re-dissolved in 2 mL methanol. Neutralized with 30 μL triethylamine, the solution was evaporated to give *N,N,N*-trimethyl-cystamine trifluoroacetate. The final product was characterized with both nuclear magnetic resonance (NMR) and mass spectroscopy (MS).

2.4 Synthesis of DOX-TPP and ADH-DOX-TPP

The synthesis of TPP-DOX was carried out as described previously. Briefly, TPP (44.8 mg), *N,N′*-dicyclohexylcarbodiimide (DCC, 24.2 mg), and *N*-hydroxysuccinimide (NHS, 13.8 mg) were dissolved in anhydrous *N,N*-dimethylformamide (DMF, 10 mL) and reacted for 4 h with stirring at room temperature. Meanwhile, DOX (50 mg) was alkalified by triethylamine (13 μL) in DMF (10 mL) and added dropwise to the activated TPP solution. This process was carried out at 0 °C for 45 min and then at room temperature overnight. The crude production was obtained by precipitation with a large amount of diethyl ether. The precipitate was dissolved in trichloromethane. After evaporation, it was extracted with deionized water to remove impurities. Finally, the DOX-TPP product was purified by silica gel thin-layer chromatography ($CHCl_3$/MeOH = 4/1, 0.5% triethylamine). DOX-TPP (80 mg) and adipic acid dihydrazide (ADH, 72 mg) were dissolved in 15 mL of anhydrous methanol. The mixture was reacted with a drop of trifluoroacetic acid with nitrogen protection overnight. After the removal of methanol under vacuum, the residue was dissolved in ethyl alcohol and centrifuged to remove unreacted ADH.

2.5 Synthesis of HA-spermine

HA-aldehyde was synthesized by mixing 100 mg HA and 50 mg sodium periodate ($NaIO_4$) in 30 mL of deionized water for 2 days at room temperature away from light. The reaction was terminated by adding 0.2 mL of ethylene glycol and stirring for 1 h, and the product was obtained by dialyzing against deionized water for 3 days, freezing, and lyophilizing. The aldehyde group in HA-aldehyde was characterized by Fourier transform infrared spectroscopy (FTIR). HA and spermine were cross-linked to form HA-spermine by coupling the aldehyde group in HA to the amino group in spermine by mixing in phosphate-buffered saline (PBS, pH 7.4, 0.1 M) for 4 h with stirring, followed by reduction with sodium cyanoborohydride for 3 days. The HA-spermine was then purified by dialysis against deionized water, frozen, and lyophilized.

2.6 Synthesis of HSTD

The carboxyl group on the HA backbone of HA-spermine was activated by 1-ethyl-3-(3-dimethylaminopropyl)-carbodiimide (EDC) and NHS in PBS (pH 5.0) for 1 h, and then the pH was adjusted to 7.4, followed by dropwise addition of DOX-TPP-ADH and *N,N,N*-trimethylcystamine with stirring overnight, and the product was purified by dialysis against deionized water, frozen and lyophilized. For blue fluorescence labeling HSTD (Blue-HSTD), HSTD, and 2-butyl(4-aminohexyl)-6-(dimethylamino)-1*H*-benz[de]isoquinoline-1,3(2*H*)-dione were dissolved in water, and EDC/NHS was then added at pH 7.0 with stirring overnight away from light. Blue-HSTD was then obtained by dialysis against deionized water, frozen, and lyophilized.

2.7 Synthesis of HA-PEI

HA-PEI conjugate was synthesized by the carbodiimide method via amide bond formation between the amine groups of branched PEI (M_W 25 kDa) and the carboxyl groups of HA (M_W 48 kDa) using EDC/NHS as coupling agent according to the reference. The weight ratio of HA to PEI was 1:5, and the product HA-PEI was obtained by dialysis against deionized water, frozen and lyophilized. The product was analyzed with mass spectrometry (Agilent 1290 HPLC-6224 Time of Flight Mass Spectrometer), ^1H and ^{13}C NMR (Bruker AVIII500M, USA) with D_2O used as a nuclear magnetic resonance (NMR) solvent (Tenglong Weibo Technology CO., Ltd. Qingdao, China), and FTIR (FIIR-4100, JASCO) in the frequency range of 4000 to 500 cm^{-1} (KBr pellet). The particle sizes and polydispersity indexes (PDI) were measured using Zetaszier Nano-S80 (Malvern Instruments, Ltd, UK). Morphologies of nanocarriers were observed under transmission electron microscopy (JEM1200EX, Japan) and cryo-TEM using a Talos™ F200C (FEI).

2.8 Preparation of HSTD/siRNA and siRNA binding study by agarose gel electrophoresis

The siRNA binding ability of the HSTD and HA-PEI was analyzed by agarose gel electrophoresis. HSTD/siRNA complexes were prepared by mixing 20 μL HSTD solution (containing polymers ranging from 0 to 15 μg) with 1 μL of negative control siRNA solution (containing 0.1 μg siRNA) and incubated for 30 min at 37 °C, after which 4 μL of RNA loading buffer was added, and the samples were loaded onto 2% agarose gels containing 0.1‰ GelRed. Electrophoresis was performed at 100 mV for 30 min in Tris-boric acid (TBA) running buffer. Nucleic acid bands were detected by ultraviolet (UV) light (312 nm). The intracellular GSH-triggering siRNA release was evaluated by incubating a series of weight ratios of HSTD to siRNA with a reductive reagent dithiothreitol (DTT) solution for 2 h followed by agarose gel electrophoresis as mentioned above.

2.9 *In vitro* release

HSTD/siTwist dissolved in PBS was transferred to cellulose membrane tubes (MWCO 8000–14,000 Da) and immersed in release medium (PBS containing 0.5% tween 80) at pH 7.4 or pH 5.0 with shaking at 37 °C away from the light. The sample was withdrawn at predetermined intervals and subjected to determination by fluorescence spectrophotometer with an excitation wave of 480 nm and emission wave of 550 nm.

2.10 Cellular uptake of siRNA

MCF-7/ADR cells were seeded into 12-well plates at a density of 5×10^4 cells/well and cultured for 24 h. After treatment, various 100 nM FAM-siRNA formulations in OPTI-MEM medium for 4 h, the cells were washed with ice-cold PBS twice, trypsinized, and

finally examined by flow cytometric analyses (FC500MCL, Beckman Coulter, USA) for siRNA determination.

2.11 Intracellular tracking of DOX-TPP or siRNA under confocal microscopy

To assess mitochondrial targeting of DOX-TPP, cells were grown on microscope slides (Thermo Scientific TM Nunc TM Lab-Tek TM II) and allowed to adhere for 24 h. Then, they were exposed to a culture medium containing 7 μM of DOX-TPP or DOX solution for 4 h. After incubation, the drug-containing solutions were removed, and 2 drops of Hoechst 33342 was added to 1 mL of RPMI 1640 medium and incubated with cells for another 30 min to stain the nucleus of the cells. The cells were then incubated with 140 nM of MitoTracker Green FM for 40 min at 37 °C. The staining solution was then removed and cells were rinsed with RPMI-1640 medium 3 times and subjected to confocal laser scanning microscopy (LSM 510 Meta, Germany). For intracellular GSH-triggered siRNA release from the HSTD/siRNA complex, the HA backbone was labeled with 2-butyl(4-aminohexyl)-6-(dimethylamino)-1*H*-benz[de]isoquinoline-1,3(2*H*)-dione (blue fluorescence molecule) to access intracellular release of siRNA or DOX-TPP from HSTD. After the cells were grown on microscope slides for 24 h, they were pretreated with GSH-Oet for 2 h or not, followed by incubation with Blue-HSTD/FAM-siRNA for another 2 h, subsequently rinsed, and subjected to confocal laser scanning microscopy as mentioned above. For assessing endosomal/lysosomal escape of HSTD/siRNA complex. Cells were grown on microscope slides for 24 h followed by incubation with HSTD/FAM-siRNA for different times (100 nM FAM-siRNA). After the incubation, the cells were washed with PBS twice and stained with 75 nM LysoTracker Blue for 1 h, then rinsed and observed under confocal microscopy. Composite images were made by overlapping the images of the individual channel.

2.12 PCR analysis

After transfection for 48 h, RNA was extracted using RNAiso Plus (TaKaRa, Japan). Reverse transcription (RT)-PCR using the PrimeScript RT-PCR Kit was performed following the manufacturer's instructions; 1 μL of the resulting cDNA was subjected to PCR reactions using specific primers. The PCR reaction was as follows: 40 cycles of 95 °C for 30 s, 95 °C for 15 s and 60 °C for 1 min. Sequences of the siTwist-1 were as follows: forward, 5'-GCA AGA UUC AGA CCC UCA ATT-3', and reverse, 5'-UUG AGG GUC UGA AUC UUG CTT-3'. Sequences of the siTwist-2 were as follows: forward, 5'-GAU GGC AAG CUG CAG CUA UTT-3', and reverse, 5'-AUA GCU GCA GCU UGC CAU CTT-3'. Sequences of the siTwist-3 were as follows: forward, 5'-GGU ACA UCG ACU UCC UCU ATT-3', and reverse, 5'-UUG AGG GUC UGA AUC UUG CTT-3'. Sequences of the glyceraldehyde 3-phosphate dehydrogenase (GAPDH) primers were as follows: forward, 5'-TTC GAC AGT CAG CCG GAT CTT C-3', and reverse, 5'-CTT CTC CAT GGT GGT GAA GAC G-3'.

2.13 Western blot analysis

Cells were collected after being transfected with siTwist for 72 h. Total cell proteins were extracted in radioimmunoprecipitation assay (RIPA) buffer (Beyotime, Shanghai, China) with 1 mM of protease inhibitors (PMSF), and concentrations were measured using the BCA-100 Protein Quantitative Analysis Kit (KeyGEN, Shanghai, China). Equal amounts of total proteins were separated in 12% sodium dodecyl sulfate (SDS) polyacrylamide gel and transferred to polyvinylidene difluoride (PVDF) membranes. The membranes were blocked in 5% nonfat dry milk in Tris-buffered saline tween-20 (TBST) for 2 h at room temperature and incubated with rabbit anti-Twist antibodies (Abcam, UK) overnight at 4 °C. After three washes with TBST, membranes were incubated with secondary antibodies (ZSGB-BIO, China) for 1 h at room temperature. An enhanced chemiluminescence detection reagent was used, and the protein bands were visualized after exposition with X-ray film. GAPDH expression was used as the housekeeping gene control. Image analyses were performed with Quantity One software.

2.14 *In vitro* cytotoxicity

The *in vitro* cytotoxicity was evaluated by 3-(4,5-dimethylthiazol-2-yl)-2,5-diphenyltetrazolium bromide (MTT) assay. Briefly, MCF-7/ADR cells were seeded at a density of 5000 cells/well into 96-well culture plates and cultured for 24 h. Cells were then exposed to RPMI 1640 medium containing free DOX, free DOX-TPP, DOX-TPP plus with PEI/siTwist (N/P = 10) complex, HSTD and HSTD/siTwist (W_t/W_t, 100/1) complex at equivalent DOX concentrations of 3, 6, 12, 25, 50 μg/mL respectively, and the concentrations of siTwist were 6, 12, 25, 50 and 100 nM correspondingly. After 6 h of incubation, the medium was replaced with fresh media and incubated for another 42 h. The medium was replaced with fresh culture medium containing MTT solution (0.5 mg/mL) followed by incubating for 4 h at 37 °C. Then, the medium was discarded and DMSO was added to dissolve the formazan crystal formed by living cells. The absorbance was measured at 570 nm using a microplate reader. Finally, the relative cell viability was calculated as follows: cell viability (%) = $(OD_{570samples} - OD_{570blank})/(OD_{570control} - OD_{570blank}) \times 100$.

2.15 *In vivo* anti-tumor assays in zebrafish model

The transgenic zebrafish model was widely used for drug evaluation, and to investigate the anti-tumor activity of drugs in a xenograft tumor model, Tg(fli1a:eGFP)+/− transgenic zebrafish were raised according to standard methods. Fertilisation was performed by photoinduced spawning over green plants and cultured at 28.5 °C in filtered tap water. Red fluorescent dye CM-DiI-labelled MCF-7/ADR cells were used in a zebrafish tumor xenograft model to allow for observation of anti-tumor effects. In brief, MCF-7/ADR cells were incubated with CM-DiI for 4 min at 37 °C, followed by 15 min at 4 °C, then were centrifuged and rinsed to remove the unincorporated dye. Two hundred trypsinized MCF-7/ADR cells were injected into the perivitelline space of dechorionated 48 hpf Tg(fli1a:eGFP)+/− transgenic zebrafish using a standard micro-injection method after zebrafish had been anesthetized with 1.85 mM of tricaine. After implantation, the zebrafish were maintained at 33 °C in Holt-Buffer solution (60 mM NaCl, 2.4 mM $NaHCO_3$, 0.9 mM $CaCl_2$, 0.67 mM KCl). Twenty-four hours after implantation, 1 nL of free DOX, HSTD, or HSTD/siTwist was injected into zebrafish at an equivalent DOX concentration of 1 mg/mL. At 4 days post-inoculation (4 dpi), the zebrafish were anesthetized with 0.62 mM of tricaine, and then live imaging was obtained using a camera (Nikon DS-Ri1)) with a microscope system (Nikon SMZ18). All experimental procedures were conducted in compliance with the directives of the animal welfare committee of Zhejiang University.

2.16 *In vivo* anti-tumor assays in mice model

Nude female BALB/c mice (4 weeks old) received a subcutaneous

injection in the right forelimb axilla with 0.1 mL of MCF-7/ADR cancer cell suspension containing 8×10^6 cells. When the tumor volume reached approximately 50 mm^3, the tumor-bearing mice were intravenously administered DOX solution and HSTD/siTwist individually (equivalent DOX concentration, 4 mg/kg) every 2 days. Eighteen days after initiation of treatment, the body weight and tumor volume were recorded, and the tumor volume was calculated as: The volume = (width^2 × length)/2. For immunohistochemical assessments, the tumor-bearing mice were intraperitoneally injected with DOX solution or HSTD/siTwist (equivalent DOX concentration, 4 mg/kg) every 3 days for a total of 8 injections. At the end of treatment, the mice were sacrificed, and tumor slices (5 μm) were cut after being frozen in an optimal cutting temperature compound (OCT) medium for the further determination of DOX localization in tumors under fluorescence microscopy. Meanwhile, blood samples were collected via the ocular vein, and liver function was evaluated by measuring the serum levels of alanine aminotransferase (ALT). The tumor and organs (heart, liver, spleen, lung, and kidney) were harvested and fixed in 4% paraformaldehyde, embedded in paraffin, sliced into 5 μm thicknesses, and then placed onto glass slides. The sections were processed with immunohistochemical analysis using a monoclonal rabbit anti-human Twist antibody, a monoclonal rabbit anti-MDR1 antibody (Abcam, Inc., Cambridge, UK), and a monoclonal rabbit anti-human Cytochrome-C antibody (CST CO., Massachusetts, USA) according to the manufacturer's instructions, hematoxylin and eosin (H&E) staining for histological study of toxicity, and terminal deoxynucleotidyl transferase-mediated dUTP nick end labeling (TUNEL) staining to detect DNA fragmentation of the nucleus in late apoptotic cells.

Then, to supplement the *in situ* tumor model, nude female BALB/c mice (4 weeks) received subcutaneous injections on the fourth pair of nipples with 0.1 mL of MCF-7/ADR cancer cell suspension containing 8×10^6 cells. When the tumor volume reached approximately 40 mm^3, the tumor-bearing mice were intravenously administered PBS, DOX solution, HSTD and HSTD/siTwist individually (equivalent DOX concentration, 4 mg/kg) every 2 days. Ten days after initiation of treatment, the body weight and tumor volume were recorded, and the tumor volume was calculated as: The volume = (width^2 × length)/2.

2.17 Statistical analysis

Statistical analyses: Data represent mean ± SD of at least three different experiments. Differences between the mean values were analyzed by two-sided unpaired Student's t-test or one-way ANOVA, and results were considered statistically significant at $P < 0.05$.

3 Results and discussion

3.1 Synthesis of HSTD

The overall synthesis route is shown in Fig. 1(a), the amino group at one end of cystamine is protected by tert-butoxycarbonyl (BOC), and the amino group at the other end is substituted by trimethyl iodomethane. Subsequently, the BOC group was removed via trifluoroacetate to obtain *N,N,N*-trimethylcystamine trifluoroacetate (Fig. S1 in the Electronic Supplementary Material (ESM)). All the peaks in ^{1}H- and ^{13}C-NMR assigned to the corresponding group of the structure (Figs. S2 and S3 in the ESM), together with Mass spectrometry (MS) characteristics (Fig. S4 in the ESM), confirmed the successful synthesis of *N,N,N*-trimethylcystamine. Meanwhile, as a lipophilic cation that could be taken up by mitochondrial membrane, triphenylphosphonium (TPP) was conjugated to DOX to achieve mitochondrial targeting of DOX as shown in our previous study [12]. DOX-TPP was then synthesized (Fig. S5 in the ESM) and characterized by MASS [M+1: 874.2986], ^{1}H-NMR (Fig. S6 in the ESM) and FTIR spectra (Fig. S7 in the ESM). As expected, the FTIR of DOX-TPP consisted of a new peak at 1656 cm^{-1}, which confirmed the formation of an amide bond (-CO-NH-) between DOX and TPP. Furthermore, DOX-TPP showed higher cytotoxicity than free DOX and the mixture of DOX and TPP in MCF-7/ADR cells (Fig. 1(b)), due to the mitochondriotropic properties of DOX-TPP. As revealed by co-localization with MitoTracker green (Fig. 1(c)), using TPP alone did not show any notable cytotoxicity within the tested concentration range.

HA is a linear polysaccharide and cannot be self-assembled in water (Fig. 2(a)). Thus, it was treated by sodium periodate to yield aldehyde functional groups (Fig. 1(a)) that were confirmed by the characteristic FTIR peak at 1733.69 cm^{-1} (stretching of C=O in the aldehyde groups) (Figs. S8(a) and S8(b) in the ESM), and subsequently substituted with spermine by aldimine condensation reaction to cross-link and form HA-spermine along with the disappearance of the characteristic FTIR peak (Fig. S8(c) in the ESM). In the meantime, we noticed that a spherical morphology (Fig. 2(b)) is favorable for the enhanced permeability and retention (EPR) effect in contrast to the linear HA (Fig. S4(a) in the ESM). Subsequently, DOX-TPP and *N,N,N*-trimethylcystamine were conjugated to the remaining carboxyl group on HA-spermine to form HSTD (Fig. 1(a)). The characteristic peaks for DOX-TPP and *N,N,N*-trimethylcystamine in ^{1}H NMR could be also observed in HSTD, indicating the formation of HSTD (Fig. S9 in the ESM). Meanwhile, the degree of *N,N,N*-trimethylcystamine, and DOX-TPP substitution, defined as the numbers of them per 100 disaccharide units of HA, was calculated to be 4.5% and 1.7%, respectively, according to elemental analysis.

3.2 Physicochemical characteristics of the HSTD/siRNA complex

In contrast to the inability of HA-spermine to form a complex with siRNA due to its negative charge (−3.12 mV), the positive charge (+3.91 mV) of HSTD (Fig. 2(c)) makes it possible to electrostatically bind to negative siRNA [13], this is also evidenced by the disappearance of nucleic acid bands in agarose gels (Fig. 2(d)). The HSTD/siRNA was well dispersed and appeared to be spherical under TEM (Fig. 2(e)) as well as Cryo-TEM (Fig. S10 in the ESM), which can image the architecture of HSTD/siRNA complex under near-native conditions [14, 15]. The size was 79.7 nm as measured by DLS (Fig. 2(f)). The release of DOX-TPP from HSTD in phosphate buffer at pH 5.0 (endosomal/lysosomal acidic pH) is faster and more than that in phosphate buffer at 7.4 (physiological pH), i.e. 85% DOX-TPP released at pH 5.0, while only 63% was released at pH 7.4 during 96 h, representing a pH-sensitive release profile due to the acid-sensitive linker (i.e. hydrazone [15]) between DOX-TPP and HA (Fig. 2(g)).

3.3 siRNA release triggered by reducing condition

The effects of different complexes on the uptake of FAM-siRNA by MCF-7/ADR cells were compared, and it was found that PEI could promote the uptake of FAM-siRNA by cells more than HSTD (Fig. 3(a)). Then, agarose gel electrophoresis was performed to evaluate

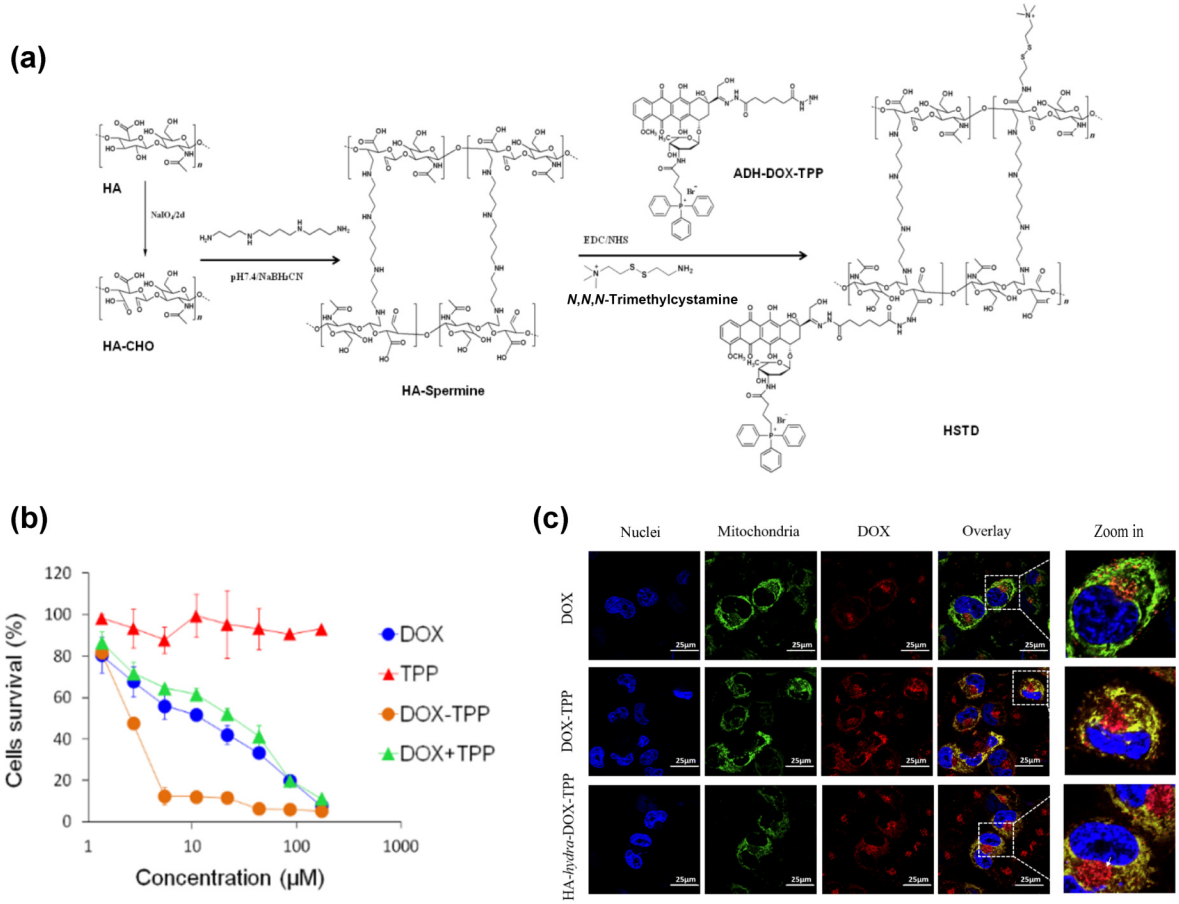

Figure 1 Cytotoxicity and intracellular distribution of DOX-TPP. (a) Synthesis process of ADH-DOX-TPP and HSTD. (b) *In vitro* cytotoxicity of free TPP, free DOX, DOX-TPP, and the mixture of TPP and DOX against MCF-7/ADR cells during 48 h as determined by the MTT assay, each value represents mean ± SD (n = 4). (c) Intracellular distribution of DOX and TPP–DOX after being incubated in MCF-7/ADR cells for 4 h, and the intracellular mitochondria were stained by MitoTracker Green followed by nuclei staining with Hoechst 33342. The cells were then observed under confocal laser scanning microscope. The overlap between the fluorescence of DOX (red) and MitoTracker (green) appears as yellow and shows the distribution of DOX in the mitochondria of cells, the scale bars represent 25 μm.

GSH-triggered cleavage of disulfide bonds in *N,N,N*-trimethylcystamine and subsequent siRNA release from HSTD with DTT used as a reducing agent. The migrations of siRNA bands were observed when HSTD/siRNA or PEI/siRNA complex was pre-treated with 50 and 200 mM DTT for 2 h [16]. Resultantly, the release of siRNA from HSTD/siRNA complex increased with the increasing DTT concentration as well as the decreasing weight ratio of HSTD to siRNA, while no band was observed for PEI/siRNA (N/P = 10) complex when either 50 or 200 mM DTT was used, which indicated a characteristic GSH-triggered release profile for HSTD/siRNA complex in the reduction environment of the cytoplasm (Fig. 3(b)).

To evaluate the intracellular GSH-triggered siRNA release, the HA backbone was labeled with blue fluorophore, with or without (i.e. control group) the 2 h pre-incubation of 20 mM GSH-Oet, an agent that could increase intracellular GSH due to its hydrolysis once in the cytoplasm, to detect the release of FAM-siRNA from blue-HSTD/FAM-siRNA. In comparison with the control group, pre-incubation of GSH-Oet could significantly promote the release of FAM-siRNA (green fluorescence) from HSTD (blue fluorescence) during 2 h, as observed by the non-localization of these two fluorescences under confocal microscope, while only part of the FAM-siRNA was separated from HSTD for the control group during 2 h, which further confirmed the GSH-responsive release of siRNA (Fig. 3(c)).

The intracellular transport and release of HSTD/FAM-siRNA were observed under the confocal microscope when endosomes/lysosomes were stained by LysoTracker Blue. Neither free DOX-TPP (red fluorescence) nor FAM-siRNA (green fluorescence) was released after 1 h (Fig. 4(a)), while some yellow spots representing the overlap of DOX-TPP (red fluorescence) and FAM-siRNA (green fluorescence) could be observed after 4 h, suggesting the endosomal/lysosomal escape of HSTD due to the proton buffering capability of spermine. After 12 h, more free FAM-siRNA (green fluorescence), as well as a small amount of DOX-TPP (red fluorescence) was released and diffused into the cytoplasm (Fig. 4(b)).

3.4 RNA interference efficiency

Being a basic helix-loop-helix transcription factor, Twist is involved in the process of EMT and then leads to drug resistance in MCF-7/ADR cells [9]. Meanwhile, HA-PEI was constructed for use as a control by grafting HA with PEI according to references [17], and the particle size is around 263 nm with a positive potential of +5 mV, which showed favorable binding ability and completely complexed siRNA at the weight ratio of 0.5 (Fig. 5(a)). Then, qRT-PCR was then used to estimate the downregulation of various sequences of siRNA on Twist mRNA expression levels in MCF-7/ADR cells using PEI as vectors, and siTwist-3 and siTwist-4 was chosen for the further studies (Fig. 5(b)). However, it was less

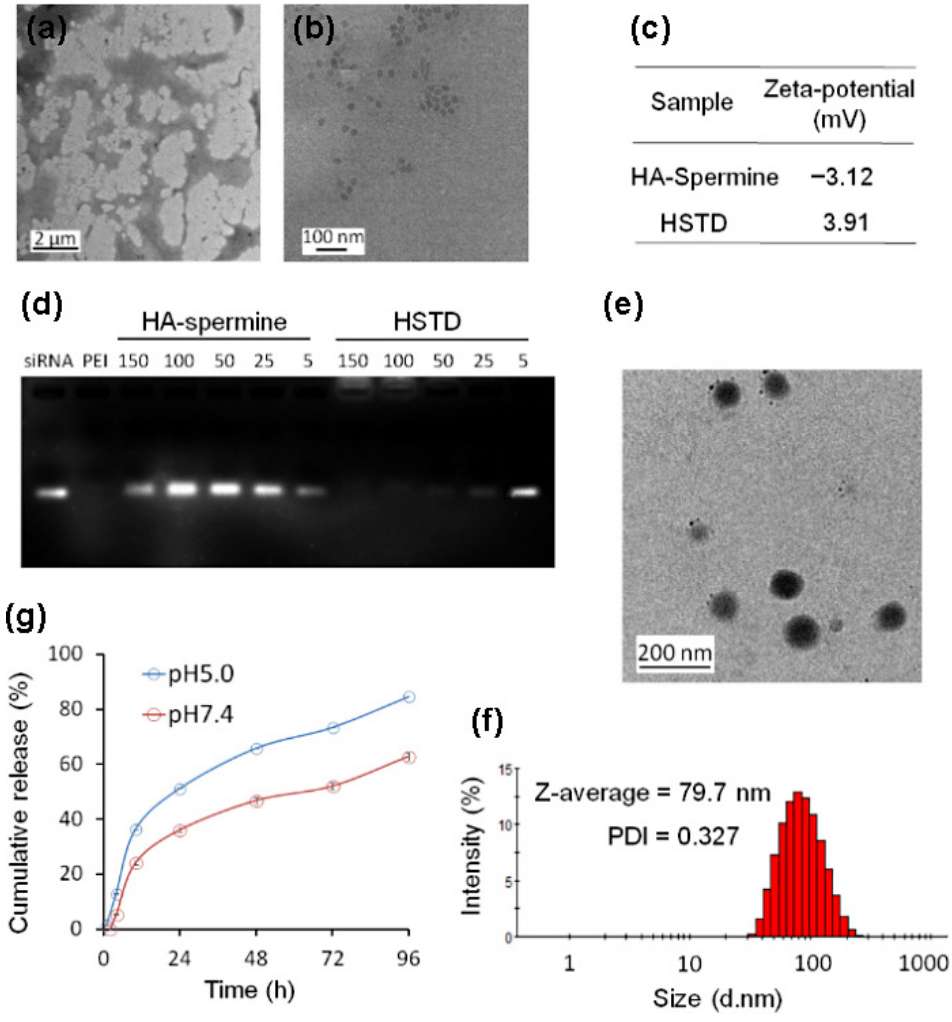

Figure 2 Characterization of HSTD. TEM images of the (a) HA (scale bar: 2 μm) and (b) HA-spermine (scale bar: 100 nm), respectively. (c) Zeta potential of HSTD and HA-Spermine. (d) Binding efficiency determined by agarose gel electrophoresis. A series of weight ratios of HSTD (or HA-PEI) to siRNA was loaded onto agarose gel with 100 ng siRNA per well. Electrophoresis was performed at a voltage of 100 V for 30 min in Tris/Borate/EDTA (TBE) buffer solution. (e) Morphology of HSTD/siRNA (W_t/W_s, 100/1) complex observed under the TEM (the scale bar is 200 nm). (f) The size distribution of HSTD/siRNA complex measured by DLS. (g) *In vitro* release of DOX-TPP from HSTD/siRNA in PBS (pH 5.0 or pH 7.4) at 37 °C during the period of 96 h.

effective in silencing Twist mRNA levels for HA-PEI/siTwist-4 (67.2%) than that of HSTD/siTwist-4 (40.1%) in MCF-7/ADR cells ($P < 0.05$) (Fig. 5(c)), indicating that the excellent binding ability with nucleic acid does not signify the remarkable transfection efficiency.

Furthermore, the successful transfection of siRNA targeting Twist can downregulate Twist expression as analyzed by western blot after 72 h of transfection. The bands were also analyzed by ImageJ software, and the Twist level was calculated as the intensity of Twist/intensity of GAPDH, and the relative level was compared to that of the scramble group. It is noticed that HSTD/siTwist could significantly reduce the Twist protein expression to 17.4% (siTwist-3) or 4.9% (siTwist-4) in MCF-7/ADR cells, respectively, which is more effective than that of PEI 25 kDa group with 62.0% for siTwist-3 and 21.5% for siTwist-4, respectively (Fig. S11 in the ESM).

3.5 Characterization of *in vitro* cytotoxicity

To determine whether MCF/ADR cells were sensitized to chemotherapeutic agents following Twist knockdown, cells were challenged with DOX, DOX-TPP and HSTD at equivalent DOX concentrations of 3, 6, 12, 25 and 50 μg/mL, respectively, together with or without siTwist transfection (Fig. 5(d)). Then, cytotoxicity assay (MTT) was performed and the half maximal inhibitory concentration (IC50) value of DOX was estimated from a plot of the percentage of viable cells versus log DOX concentration. Mitochondria-targeted DOX-TPP resulted in a higher cytotoxicity (IC50, 18.81 μg/mL) than that of DOX solution (IC50, 54.45 μg/mL) in MCF-7/ADR cells. Then, the cells were exposed to DOX-TPP plus PEI 25kDa mediated siTwist transfection, which showed significantly higher cytotoxicity (IC50, 9.27 μg/mL) than DOX-TPP alone without siTwist transfection, while PEI alone did not show any notable cytotoxicity within the tested concentration range, indicating a significantly increased sensitivity of MCF-7/ADR cell toward DOX due to knockdown of Twist expression. However, neither DOX-TPP nor PEI could be used *in vivo* due to the off-target as well as toxicity caused by positive potential, then HA was employed to construct the nanocarrier (HSTD) due to its biocompatibility and selectivity to tumor cells (i.e. MCF-7) that overexpress CD44, and HSTD represents slightly higher cytotoxicity (IC50, 14.10 μg/mL) in comparison with DOX-TPP.

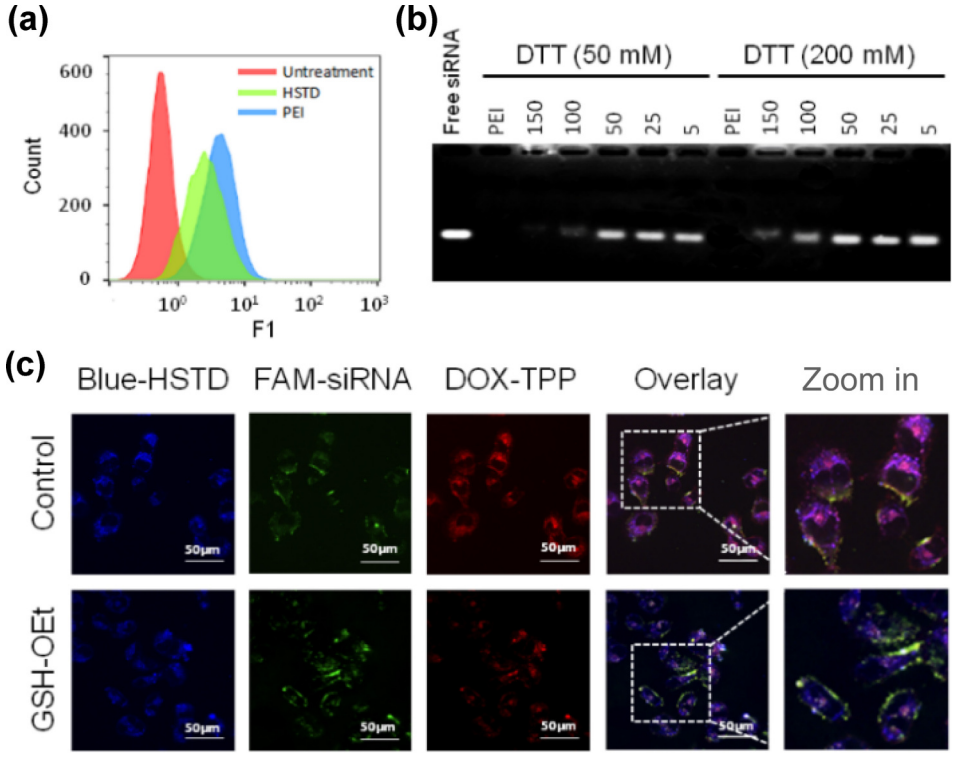

Figure 3 GSH triggered siRNA release and intracellular lysosome escaping of the HSTD/siRNA complex. (a) Cellular uptake of FAM-siRNA in MCF-7/ADR cells mediated by PEI and HSTD (200 nM/well siRNA). (b) Agarose gel electrophoresis retardation assay of HSTD/siRNA complex (weight ratios of HSTD to siRNA ranging from 5 to 150) pre-treated with different concentrations of DTT solution for 2 h at 37 °C. (c) Intracellular GSH triggered siRNA release from HSTD/FAM-siRNA complex after pre-incubation with 20 mM GSH-Oet for 2 h or not.

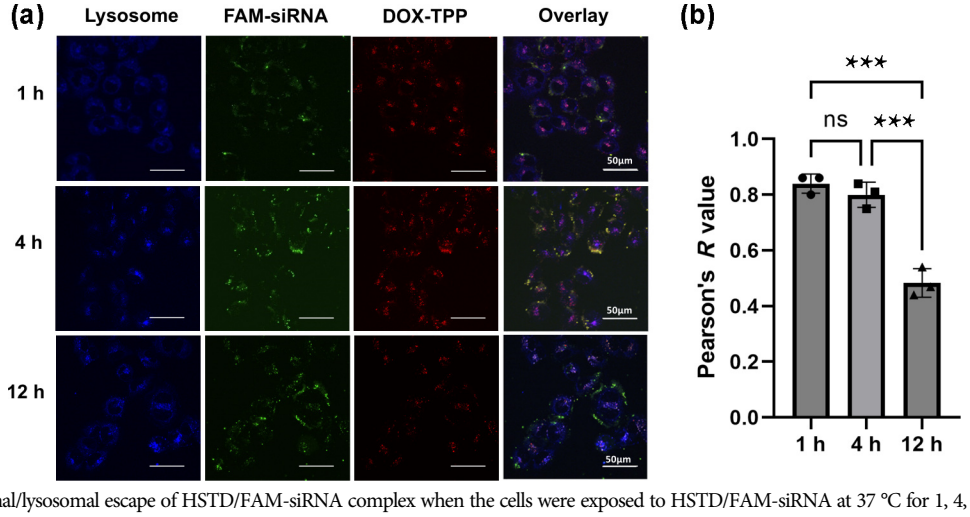

Figure 4 (a) Endosomal/lysosomal escape of HSTD/FAM-siRNA complex when the cells were exposed to HSTD/FAM-siRNA at 37 °C for 1, 4, or 12 h, lysosome were stained by LysoTracker Blue and were then observed under confocal laser scanning micrographs. (b) Quantification of the overlap between FAM-siRNA and DOX-TPP over time by Image J ($n = 3$; ns, $P > 0.05$; *$P < 0.05$; **$P < 0.01$; ***$P > 0.001$).

Moreover, significantly higher cytotoxicity (IC50, 9.84 μg/mL) could be observed when combined with siTwist transfection for HSTD/siTwist treatment. These results indicated that the co-delivered siTwist could sensitize drug-resistant MCF-7/ADR cells to chemotherapeutic agents in a single nano-drug delivery system (i.e. HSTD).

3.6 *In vivo* anti-tumor assays in zebrafish model

To investigate the toxicity of DOX toward MCF-7/ADR cells *in vivo*, a zebrafish xenograft experiment was employed, as it offers a rapid and efficient approach for assessing drug effects on human cancer cells at various stages of tumorigenesis because of its *in vivo* visualization of cell migration and cell mass formation and interaction between human cancer and zebrafish cells in the transparent animal under microscopy observation [18]. Therefore, MCF-7/ADR cells were labeled with a fluorescent tracking dye (CM-DiI) and injected into the zebrafish perivitelline space. Then they proliferated and formed masses primarily in the regions surrounding the intestine, pancreas, and liver (1 day post-inoculation (dpi)). After drug treatment for 3 days (4 dpi), anti-

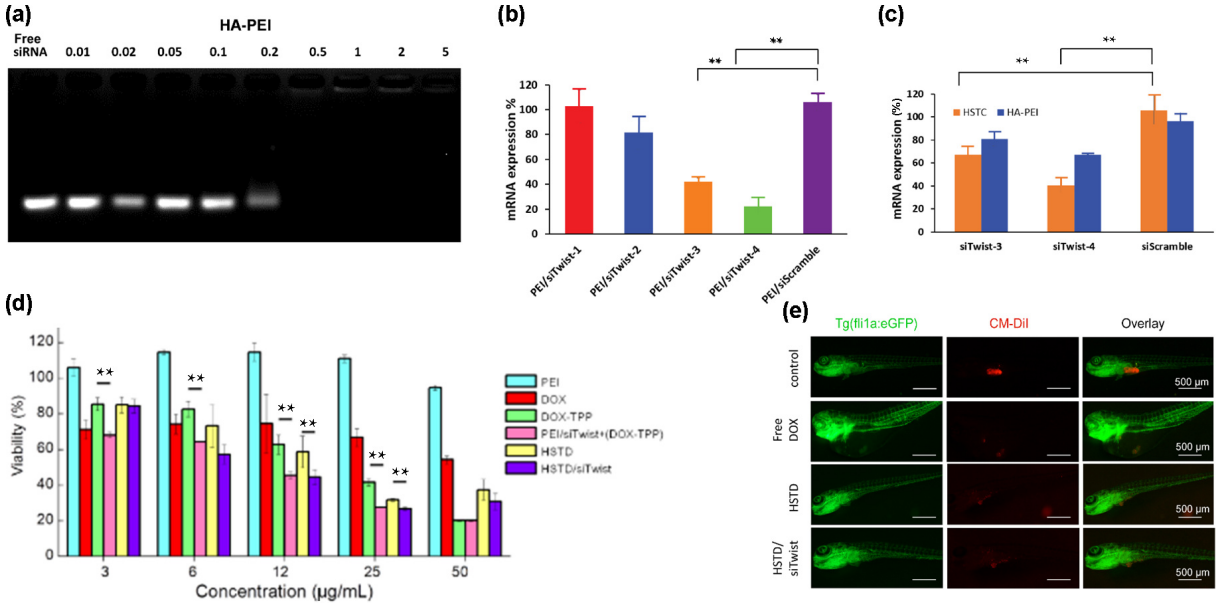

Figure 5 Effect of HSTD/siRNA in MCF-7/ADR cells and Tg(fli1a:eGFP)+/- transgenic zebrafish tumor model. (a) Agarose gel electrophoresis retardation assay of HA-PEI with different weight ratios to siRNA. (b) and (c) Expression levels of Twist mRNA in MCF-7/ADR cells measured by real-time PCR analysis after transfection with 200 nM siTwist mediated by PEI, HA-PEI, or HSTD. $^{**}P < 0.01$ ($n = 5$). (d) *In vitro* cytotoxicity of free PEI, free DOX, free DOX-TPP, DOX-TPP combined with PEI/siTwist (N/P = 10) complex, HSTD, and HSTD/siTwist (W_i/W_t, 100/1) in MCF-7/ADR cells after application on cells for 48 h. Each value represents the mean and SD ($n = 4$). **represents a significant difference ($P < 0.01$). (e) Anti-tumor activities in transgenic zebrafish models. Red fluorescent dye CM-DiI-labelled MCF-7 cells were injected in Tg(fli1a:eGFP)+/– transgenic zebrafish. 1 nL of free DOX, HSTD, and HSTD/siTwist complex was injected into zebrafish at an equivalent DOX concentration of 1 mg/mL. At 4 days post-inoculation (4 dpi), the zebrafish were imaged by a camera (Nikon DS-Ri1) with a microscope system (Nikon SMZ18) for live imaging (PE is the abbreviation for pericardial edema).

tumor effects were observed in the free DOX, HSTD, and HSTD/siTwist groups in contrast to the control group, which had not been treated with the drug. In the MCF-7/ADR tumor model, the control group formed solid tumors, and the HSTD/siTwist group inhibited tumor growth more effectively than the free DOX group. Particularly, an increased volume of ventricle, together with body distortion, could be observed for the free DOX group, indicating that cardiotoxicity is mediated by DOX, while HSTD and HSTD/siTwist may decrease side effects (i.e. cardiotoxicity) (Fig. 5(e)).

3.7 *In vivo* anti-tumor assays in mice model

Many tumor cells (i.e. MCF-7/ADR) overexpress HA-binding receptors, such as CD44. Then, coating the nanocarrier with HA, together with the enhanced permeability and retention (EPR) effect, may contribute to the stronger DOX fluorescence in tumor slices for HSTD/siTwist compared to that of the DOX solution group in nude mice bearing MCF-7/ADR tumors (Fig. S12 in the ESM).

The tumor volumes and body weights were measured every 2 days up to 18 days to evaluate the *in vivo* anti-tumor efficacy of HSTD/siTwist in nude mice bearing MCF-7/ADR tumors (Figs. 6(a) and 6(b)). It is noticed that tumors in mice receiving HSTD/siRNA solution grew up to 304.9 mm^3 and were significantly smaller than those in mice that received free DOX solution (485.13 mm^3), while the tumor volume was as large as 674.47 mm^3 for the control group (PBS treatment), demonstrating that HSTD/siRNA exhibited a favorable anti-tumor effect *in vivo*. In addition, the body weights decreased gradually during the injection with free DOX (−2%) due to the serious side effects of DOX as mentioned in the above zebrafish xenograft studies, while mice treated with HSTD/siTwist showed slightly increased body weights (+1.74%). At the same time, results of the *in situ* tumor model showed that both HSTD and HSTD/siTwist showed better tumor inhibition effects than free DOX, but maybe due to the lower growth rate of the in situ tumors, the growth space was not enough to clearly show the difference between the HSTD and HSTD/siTwist groups (Fig. S13 in the ESM).

Immunohistochemical assays were performed to evaluate the expression of both Twist and P-glycoprotein (P-gp) in tumor tissues of MCF-7/ADR-bearing nude mice after different treatments. Cell nuclei were stained blue, and the brown blots indicated the Twist and P-gp expression in the tumor tissue (Fig. 6(c)). Treatment with DOX alone led to the highest level of P-gp expression because the transient exposure of the cells to chemotherapeutic drugs that could induce P-gp expression, which is also involved in EMT and Twist suppression, could inhibit the drug-induced P-gp expression, concomitant with reduction in resistance to chemotherapeutic drugs [19]. As expected, expression of the Twist and P-gp protein in tumor tissues was effectively downregulated by HSTD/siTwist in contrast to the DOX group. Moreover, cytochrome C involved in the apoptosis process [20] was expressed at the highest level in tumor tissues from mice receiving HSTD/siTwist, as well as the most prominent cancer-cell apoptosis revealed by TUNEL assay, indicating that the co-delivered chemotherapeutic drugs and siTwist acted synergistically on MCF-7/ADR cells to induce apoptosis *in vivo* (Fig. 6(c)).

Histological analysis of H&E stained sections of main organs and tumor tissue was next performed (Fig. S14 in the ESM). Cardiomyocytes were slightly sparse and unevenly arranged in the mice treated with free DOX, pointing to myocardial cell damage induced by DOX, which limits its clinical application. By contrast, HSTD/siTwist showed no obvious histopathological abnormality in the myocardium due to encapsulation of chemotherapeutic drugs in HA nanocarriers and consequently altered *in vivo*

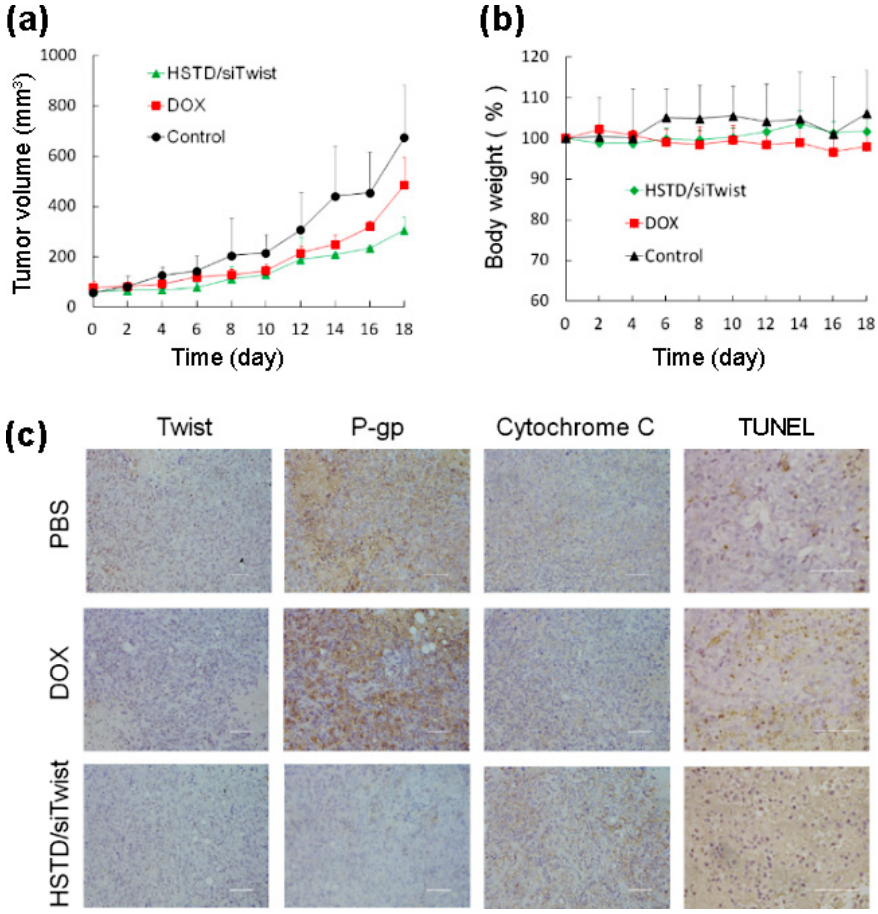

Figure 6 Anti-tumor effects in nude mice bearing MCF-7/ADR tumors after being treated with DOX and HSTD/siTwist complex. (a) Tumor growth and (b) body weight curves after intravenous administration of DOX solution and HSTD/siRNA on nude mice bearing MCF-7/ADR tumors every 2 days for 9 times at a dosage of 4.0 mg/kg of DOX (n = 6) when the tumor reached a size of 50 mm^3 (n = 5), and (c) representative images of immunohistochemical staining of xenografted tumors, including Twist, P-gp, Cyt-C and TUNEL assay (×20), scale bars: 100 μm.

pharmacokinetics and biodistribution. The liver is the main organ for metabolism in the body, and the normal liver tissue sections showed regular cell arrangements and visible nuclei, while the cells were necrotic for the mice receiving DOX solution. By contrast, mice in the HSTD/siTwist group had normal liver cells, and the nuclei were clear and showed non-toxicity to other organs (i.e. spleen, lung, and kidney), which demonstrated its biocompatibility *in vivo*. H&E stained tumor sections for the control group treated with PBS showed obvious nuclear polymorphism and growth inhibition could be observed in tumor tissues for the HSTD/siTwist groups, which resulted in a higher level of tumor necrosis than that of the DOX group. These results indicate favorable biocompatibility and antitumor effectivity of HSTD/siTwist for application both *in vitro* and *in vivo*.

4 Conclusions

In conclusion, we constructed the HSTD nanocarrier co-delivering chemotherapeutic DOX-TPP and siTwist. This novel hyaluronic acid nanocarrier can accumulate in the mitochondria and cause cell apoptosis, while *N,N,N*-trimethylcystamine may be broken down by GSH, releasing free siRNA rapidly and completely, and consequently resulting in excellent transfection efficiency. With good anti-tumour effects and biocompatibility, we believe that HSTD provides a vital addition to the existing dedication to identifying high transfection nanocarriers.

Electronic Supplementary Material: Supplementary material (further details of the synthesis parh, NMR, FTIR, MS, the anti-tumor results in *in situ* model) is available in the online version of this article at https://doi.org/10.26599/NR.2025.94907076.

Data availability

All data needed to support the conclusions in the paper are presented in the manuscript and the Electronic Supplementary Material. Additional data related to this paper may be requested from the corresponding author upon request.

Acknowledgements

This work was supported by the National Key Research and Development Program of China (No. 2022YFE0107800), National Natural Science Foundation of China (Nos. 82373206, and 82073332), and Zhejiang Provincial Natural Science Foundation of China (No. LHDMZ24H300002). We thank Mengjie Yu at Bio-Ultrastructure Analysis Lab. of Analysis Center of Agrobiology and Environmental Sciences, Zhejiang University for her technical assistance on transmission electron microscopy; Jianyang Pan (Research and Service Center, College of Pharmaceutical Sciences, Zhejiang University) for performing NMR spectrometry for structure elucidation; Yingying Huang at Zhejiang University School of Medicine for her technical assistance on flow cytometry;

Qin Han, Chenyu Yang and Dandan Song at the Center of Cryo-Electron Microscopy (CCEM), Zhejiang University for their technical assistance on confocal laser scanning microscopy and transmission electron microscopy; Junli Xuan and Yanwei Li at the Core Facilities of Zhejiang University School of Medicine for technical assistance of confocal laser scanning microscopy and flow cytometry analysis.

Declaration of competing interest

All the contributing authors report no conflict of interests in this work.

Author contribution statement

R.-L. J. and H.-N. L.: Experimental design, project administration and writing manuscript. Y.-F. Y.: Data curation. Z.-C. Z., and Q. D.: Experimental design and revising manuscript. X.-Y. B. and L.-J. W.: Data curation and revising manuscipt. Y.-X. Q. and X. T.: Experimental design. X.-Y. S., X.-F. Y., and Z.-Q. B.: Data curation. M. H.: Funding acquisition, project administration, revising manuscipt and supervision. All the authors have discussed the results and approved the final manuscript.

Informed consent

Not applicable.

Ethics statement

The animal experiments were approved by the Institutional Animal Care and Use Committee (IACUC) of Zhejiang University, and we have complied with all relevant ethical regulations (Ethical code: ZJU20240344).

Use of AI statement

None.

References

[1] Graça, M. F. P.; Miguel, S. P.; Cabral, C. S. D.; Correia, I. J. Hyaluronic acid-based wound dressings: A review. *Carbohydr. Polym.* **2020**, *241*, 116364.

[2] Vasvani, S.; Kulkarni, P.; Rawtani, D. Hyaluronic acid: A review on its biology, aspects of drug delivery, route of administrations and a special emphasis on its approved marketed products and recent clinical studies. *Int. J. Biol. Macromol.* **2020**, *151*, 1012–1029.

[3] Kim, H.; Lee, S.; Ki, C. S. Modular formation of hyaluronic acid/β-glucan hybrid nanogels for topical dermal delivery targeting skin dendritic cells. *Carbohydr. Polym.* **2021**, *252*, 117132.

[4] Liang, Y.; Wang, Y. H.; Wang, L. P.; Liang, Z. J.; Li, D.; Xu, X. Y.; Chen, Y. B.; Yang, X. C.; Zhang, H. B.; Niu, H. T. Self-crosslinkable chitosan-hyaluronic acid dialdehyde nanoparticles for CD44-targeted siRNA delivery to treat bladder cancer. *Bioact. Mater.* **2021**, *6*, 433–446.

[5] Lee, Y.; Shinn, J.; Xu, C.; Dobson, H. E.; Neamati, N.; Moon, J. J. Hyaluronic acid-bilirubin nanomedicine-based combination chemoimmunotherapy. *Nat. Commun.* **2023**, *14*, 4771.

[6] Yin, T. J.; Wang, L.; Yin, L. F.; Zhou, J. P.; Huo, M. R. Co-delivery of hydrophobic paclitaxel and hydrophilic AURKA specific siRNA by redox-sensitive micelles for effective treatment of breast cancer. *Biomaterials* **2015**, *61*, 10–25.

[7] Liu, L. X.; Cao, F. Q.; Liu, X. X.; Wang, H.; Zhang, C.; Sun, H. F.; Wang, C.; Leng, X. G.; Song, C. X.; Kong, D. L. et al. Hyaluronic acid-modified cationic lipid-PLGA hybrid nanoparticles as a nanovaccine induce robust humoral and cellular immune responses. *ACS Appl. Mater. Interfaces* **2016**, *8*, 11969–11979.

[8] Sahiner, N.; Sagbas, S.; Sahiner, M.; Ayyala, R. S. Polyethyleneimine modified poly(Hyaluronic acid) particles with controllable antimicrobial and anticancer effects. *Carbohydr. Polym.* **2017**, *159*, 29–38.

[9] Hashemi, M.; Hajimazdarany, S.; Mohan, C. D.; Mohammadi, M.; Rezaei, S.; Olyaee, Y.; Goldoost, Y.; Ghorbani, A.; Mirmazloomi, S. R.; Gholinia, N. et al. Long non-coding RNA/epithelial-mesenchymal transition axis in human cancers: Tumorigenesis, chemoresistance, and radioresistance. *Pharmacol. Res.* **2022**, *186*, 106535.

[10] Kim, M.; Lee, J. S.; Kim, W.; Lee, J. H.; Jun, B. H.; Kim, K. S.; Kim, D. E. Aptamer-conjugated nano-liposome for immunogenic chemotherapy with reversal of immunosuppression. *J. Control. Release* **2022**, *348*, 893–910.

[11] Liu, H. N.; Guo, N. N.; Guo, W. W.; Huang-Fu, M. Y.; Vakili, M. R.; Chen, J. J.; Xu, W. H.; Wei, Q. C.; Han, M.; Lavasanifar, A. et al. Delivery of mitochondriotropic doxorubicin derivatives using self-assembling hyaluronic acid nanocarriers in doxorubicin-resistant breast cancer. *Acta Pharmacol. Sin.* **2018**, *39*, 1681–1692.

[12] Han, M.; Vakili, M. R.; Soleymani Abyaneh, H.; Molavi, O.; Lai, R.; Lavasanifar, A. Mitochondrial delivery of doxorubicin via triphenylphosphine modification for overcoming drug resistance in MDA-MB-435/DOX cells. *Mol. Pharmaceutics* **2014**, *11*, 2640–2649.

[13] Han, M.; Lv, Q.; Tang, X. J.; Hu, Y. L.; Xu, D. H.; Li, F. Z.; Liang, W. Q.; Gao, J. Q. Overcoming drug resistance of MCF-7/ADR cells by altering intracellular distribution of doxorubicin via MVP knockdown with a novel siRNA polyamidoamine-hyaluronic acid complex. *J. Control. Release* **2012**, *163*, 136–144.

[14] Scherr, J.; Parey, K.; Klusch, N.; Murphy, B. J.; Balser, S.; Neuhaus, A.; Zickermann, V.; Kühlbrandt, W.; Terfort, A.; Rhinow, D. Self-perforated hydrogel nanomembranes facilitate structural analysis of proteins by electron cryo-microscopy. *ACS Nano* **2017**, *11*, 6467–6473.

[15] Karimi, M.; Ghasemi, A.; Sahandi Zangabad, P.; Rahighi, R.; Moosavi Basri, S. M.; Mirshekari, H.; Amiri, M.; Shafaei Pishabad, Z.; Aslani, A.; Bozorgomid, M. et al. Smart micro/nanoparticles in stimulus-responsive drug/gene delivery systems. *Chem. Soc. Rev.* **2016**, *45*, 1457–1501.

[16] Yeh, P. H.; Sun, J. S.; Wu, H. C.; Hwang, L. H.; Wang, T. W. Stimuli-responsive HA-PEI nanoparticles encapsulating endostatin plasmid for stem cell gene therapy. *RSC Adv.* **2013**, *3*, 12922–12932.

[17] Ganesh, S.; Iyer, A. K.; Morrissey, D. V.; Amiji, M. M. Hyaluronic acid based self-assembling nanosystems for CD44 target mediated siRNA delivery to solid tumors. *Biomaterials* **2013**, *34*, 3489–3502.

[18] Yang, J.; Shimada, Y.; Olsthoorn, R. C. L.; Snaar-Jagalska, B. E.; Spaink, H. P.; Kros, A. Application of coiled coil peptides in liposomal anticancer drug delivery using a zebrafish xenograft model. *ACS Nano* **2016**, *10*, 7428–7435.

[19] Mirzaei, S.; Abadi, A. J.; Gholami, M. H.; Hashemi, F.; Zabolian, A.; Hushmandi, K.; Zarrabi, A.; Entezari, M.; Aref, A. R.; Khan, H. et al. The involvement of epithelial-to-mesenchymal transition in doxorubicin resistance: Possible molecular targets. *Eur. J. Pharmacol.* **2021**, *908*, 174344.

[20] Ali, M. R. K.; Rahman, M. A.; Wu, Y.; Han, T. G.; Peng, X. H.; Mackey, M. A.; Wang, D. S.; Shin, H. J.; Chen, Z. G.; Xiao, H. P. et al. Efficacy, long-term toxicity, and mechanistic studies of gold nanorods photothermal therapy of cancer in xenograft mice. *Proc. Natl. Acad. Sci. USA* **2017**, *114*, E3110–E3118.